Submitted to *Journal of Geophysical Research*, 2000.

POLAR observations and model predictions during May 4, 1998, magnetopause, magnetosheath and bow shock crossings

P. Song[1,2], J. U Kozyra[1], M. O. Chandler[3], C. T. Russell[4], W. K. Peterson[5], K. J. Trattner[5], R. H. W. Friedel[6], J.-H. Shue[7], T. E. Moore[8], K. W. Ogilvie[8], R. P. Lepping[8], D. J. McComas[6]

1. Space Physics Research Laboratory, Department of Atmospheric, Oceanic and Space Sciences, University of Michigan, Ann Arbor

2. Now at Department of Environmental, Earth and Atmospheric Science and Center for Atmospheric Research, University of Massachusetts, Lowell

3. NASA Marshall Space Flight Center, Huntsvill, AL

4. Institute of Geophysics and Space Physics, University of California, Los Angeles

5. Lockheed-Martin Corp., Palo Alto, CA

6. Los Alamos National Laboratory, Los Alamos, NM

7. Applied Physics Laboratory, The Johns Hopkins, Laurel, MD

8. NASA Goddard Space Flight Center, Greenbelt, MD

Abstract. During the rise to the maximum phase of solar cycle 23, several periods of extreme solar wind conditions have occurred. During such an example on 4 May 1998, the solar wind monitors observed a period of strong southward interplanetary magnetic field (IMF) accompanied by a solar wind dynamic pressure that was 30 times higher than average. During this period, the POLAR spacecraft crossed the magnetopause and bow shock and experienced its first solar wind encounter. This case provides a rare opportunity to study the magnetopause, low-latitude boundary layer (LLBL), magnetosheath, and bow shock and to test our ability to model the dynamic behavior of these boundary regions under extreme and highly variable solar wind conditions. In this study, we use the gas dynamic convected field model (GDCF) to predict the time-dependent magnetic field and plasma properties upstream from the magnetopause and the location of the POLAR spacecraft relative to the magnetopause and bow shock during the event.

1. Abstract - continued

To test the accuracy of the prediction, model magnetic field characteristics are compared to the fields observed along the satellite track by the magnetometer on POLAR. The predicted model plasma characteristics (density, velocity and temperature) are compared to moments derived from TIDE observations, extrapolated to account for the higher energy portion of the magnetosheath distributions. Where ambiguities occur in identifying the satellite location, plasma distribution functions from two additional ion detectors (TIMAS and HYDRA) are used to resolve the observed location of POLAR relative to the boundaries. With this procedure, carried out separately for ACE and WIND and for two different magnetopause models, observed

features at POLAR can be traced back to drivers in the solar wind, providing a unique opportunity to assess the evolution of the solar wind and its predictability from the solar wind monitors to the magnetopause. When the POLAR apogee drifts to low latitudes in the future, it will provide more and more observations in this region. Therefore, what we learn from this case can be indicative of what we will see in the future in POLAR operations. The high level correlation between the predictions and in situ measurements indicates that the solar wind monitors often provide adequate and useful solar wind conditions near the earth. The tests indicate that in this event, the vacuum dipole field magnetosphere model predicts a significantly larger magnetosphere than observed. While the empirical magnetopause model predictions are more consistent with the observations, they over-predict the response of the magnetosphere to transient southward turnings of the IMF; indicating that the magnetosphere does not respond to the southward IMF turnings on small time scales. Sometimes, there are significant differences at relatively small time scales between the measurements from the two solar wind monitors. It is possible for the solar wind conditions near the earth to be different from the measurements made by at least one of the solar wind monitors. Cautions should be taken when interpreting near earth observations if the observations are inconsistent at small time scales with the predictions based on one solar wind monitor.

2. Introduction

On May 4, 1998, large disturbances occurred in the solar wind. The solar wind dynamic pressure reached as high as 60 nPa, 30 times higher than that of the average solar wind. Furthermore, there were extended periods of strong southward interplanetary magnetic field (IMF). During this event, the magnetopause experienced the largest erosion on record [*Russell et al.*, 2000]. POLAR experienced its first dayside low-latitude magnetopause crossings, bow shock crossings and encounters with the solar wind. There were two solar wind monitors available during the event which provide solar wind measurements at two different upstream locations. In this study, we combine the information obtained from POLAR and the two solar wind monitors with the knowledge we accumulated about the magnetopause and magnetosheath over the past few years. The purpose of this study is three fold. First, we use this rare occasion to verify the sheath model that has been developed recently [*Spreiter and Stahara*, 1980; *Song et al.*, 1999a, b]. Second, we verify magnetopause models [*Spreiter and Stahara*, 1980; *Shue et al.*, 1998] under large amplitude variations. In particular, we examine the dependence on north-south component (B_Z) of the IMF in the models. Last, we provide a reference location of POLAR and examine the correlation of the upstream variations with POLAR observations for other studies of this event.

To determine the location of POLAR with respect to the magnetospheric boundaries, there are a few challenges. The first is to determine the location of the magnetopause which moves with the changes in the upstream conditions. During the event, very large-amplitude, short-time scale changes in the upstream solar wind were observed. When the magnetopause moved very fast over large distances in response to these rapid large-amplitude variations, POLAR changed its location relative to the magnetopause quickly, even though the satellite moved slowly in space. The satellite might sample very different regions in space in a very short-time period. Second, similar to the magnetopause, the bow shock also moved back and forward rapidly. Its location depends on the location of the magnetopause and solar wind Mach number. Third, the travel times to POLAR of the solar wind features, observed by the two solar wind monitors, may vary during periods when the solar wind changed its speed and direction and when the solar wind features evolved and changed their orientation.

Solar wind measurements from both WIND [*Ogilvie and Parks*, 1996] and ACE [*McComas et al.*, 1998; *Smith et al.*, 1998] provide the basis for determining the location of the magnetopause. We then employ the gas dynamic convected field (GDCF) model [Spreiter and Stahara, 1980] to calculate the location of the bow shock and the field and plasma parameters in the magnetosheath. We extract the model values of the magnetosheath parameters along the POLAR satellite trajectory and compare them with the POLAR observations. This scheme takes into account most of the dynamic processes that have time scales longer than the magnetosheath wave transient time, which is of the order of one minute. In the model predictions, the solar wind arrival time changes as the solar wind velocity changes, and the magnetopause and bow shock locations vary as the upstream conditions change. These three effects are handled in a systematic manner. The dynamics that is not included in the scheme involves waves with time scales of the order of the Alfven transient time, such as wave reflections at the bow shock, and the magnetopause and in the magnetosphere, and quasi-steady state wave fronts of non-fast modes [*Song*

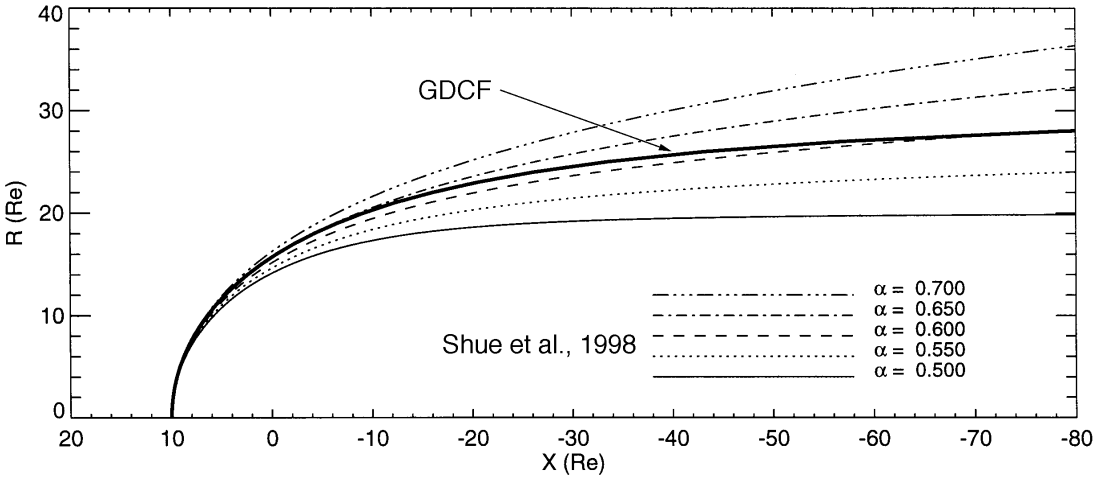

Figure 1. Comparison of the shapes of the magnetopause with gas dynamics form of $\cos^2\psi$ (think line) and *Shue et al.* [1998] (thin lines of various styles). The gas dynamic form corresponds to the *Shue et al.* [1998] model with $\alpha = 0.65$ on the dayside.

et al., 1999a, b]. We assume that the magnetosphere responds in unison instantaneously to every solar wind variation as it hits the magnetopause. Details of the justification of the method and the physical implications associated with the assumptions employed in the method can be found in *Song et al.* [1999a, b].

In addition to the tests made in *Song et al.* [1999a, b], we further examine the effects of different magnetopause models. In the standard GDCF model, the magnetopause standoff distance is determined by the balance between the solar wind dynamic pressure and a vacuum magnetospheric dipole field. The standoff distance drops roughly with a -1/6 power law dependence on the solar wind dynamic pressure. Based on large databases of magnetopause crossings, several quantitative predictive empirical magnetopause models have been developed in recent years [*Roelof and Sibeck*, 1993; *Petrinec and Russell*, 1996; *Shue et al.*, 1998; *Kuznetsov and Suvorova*, 1998]. Some of the empirical models cannot be used under extreme solar wind conditions and others have been tested extensively [*Shue et al.*, 2000].

In this study we test the *Shue et al.* [1998] model because of its simplicity in mathematical forms and desirable behavior under extreme solar wind conditions [*Shue et al.*, 2000]. The standoff distance in the *Shue et al.* [1998] model depends on both the solar wind dynamic pressure and the north-south component of the IMF. The solar wind dynamic pressure effect which shows a power law -1/6.6 dependence may partially reflect the effects of the ring current. The IMF B_Z dependence reflects the effects of reconnection at the magnetopause and to some extent the effects of field-aligned currents. The shape of the magnetopause in the *Shue et al.* [1998] model is specified by a functional form of $(1+\cos\theta)^{-\alpha}$ where θ is the solar zenith angle and α is a function of solar wind pressure and IMF B_Z. However, the shape of the magnetopause used in the GDCF model has a form of $\cos^2\psi$, where ψ is the angle between the solar wind direction and the normal to the magnetopause surface. This form is based on the gas dynamic semi-empirical expression for a supersonic flow [*Spreiter and Stahara*, 1980] (see more detailed discussion by *Petrinec and Russell* [1995]). In this study, we test two different standoff-distance models, one derived from the dipole field model and the other from the *Shue et al.* [1998] model while using the shape of the magnetopause built in the GDCF model. The difference in the shape between the GDCF and Shue et al. models is shown in Figure 1. In a very large spatial region, the shape derived from the GDCF model is similar to that from *Shue et al.* [1998] with α being equal to 0.6. It is not a coincidence that the average value of α in the database of *Shue et al.* [1998] is near 0.6: the dayside magnetosphere does act like an aerodynamical obstacle to a supersonic flow. For the event studied in this work, the solar zenith angle is within 45°.

Figure 2 shows the solar wind measurements from ACE (solid lines) and WIND (dashed lines) during the

period in which we are interested. The solar wind was fast, nearly double its average speed. The solar wind was denser than normal conditions. Furthermore, there were a few very strong density enhancements, which led to enhancements in the solar wind dynamic pressure to more than 8 times higher. During the interval, the IMF was stronger than usual and the z component fluctuated on about a 20-min time scale. ACE was at (227, -32, -17)R_E GSE and WIND was at (214, 7, 27)R_E GSE. Although the two satellites were separated by less than 50 R_E across the sun-earth line, there are significant differences in the timings of some features. Furthermore some features appeared quite different at the two locations. For example, near 0640 UT, as highlighted by a horizontal bar, the scales of the feature shown in B_Z are quite different. These differences will create distinct differences in the predictions which are useful when evaluating the performance of the predictions. Notice that ACE was closer to the stagnation streamline than WIND when including the Earth's orbital motion. As will be seen in the results, the features observed by POLAR are more likely to be those recorded by ACE during the interval that we present in this study.

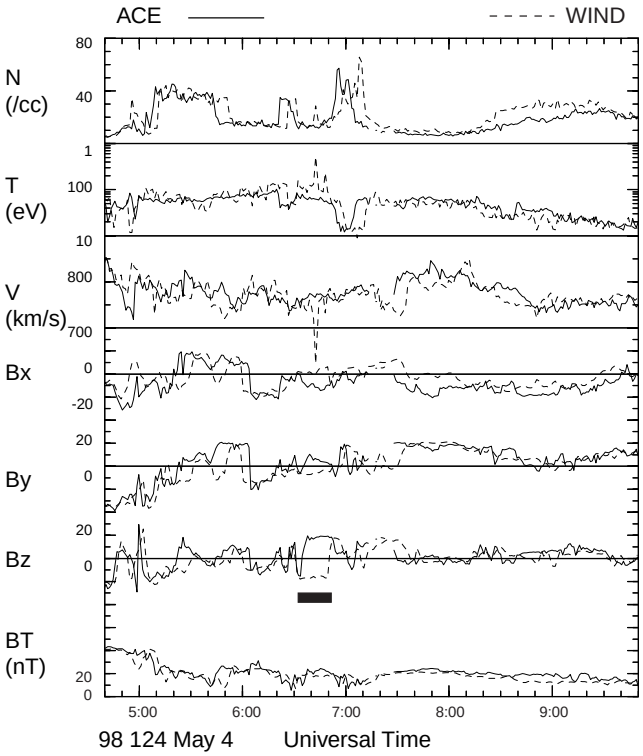

Figure 2. Solar wind/IMF measurements by WIND (dashed lines) and ACE (solid lines). The quantities shown from the top are ion number density in cm^{-3}, ion temperature in K degrees, ion velocity in km/s, and the three components in GSE and the magnitude of the magnetic field. Highlighted by a horizontal bar is a period when the two monitors measured an opposite B_Z.

3. Prediction of Magnetosheath Quantities

Figure 3 compares the POLAR observations (solid lines) with the GDCF model predictions (dashed lines) using the WIND solar wind data and the vacuum dipole field model to set the standoff distance. Let us first examine the observations. The plasma moments are taken from the Thermal Ion Dynamic Experiment (TIDE) [*Moore et al.*, 1995]. TIDE was designed to provide three-dimensional ion measurements from 0 to 500 eV. The instrument was under a complicated operational mode during the event. It combined all signals in the elevation directions into a single record. Therefore, the measurements are equivalent to those from a wide angle two-dimensional detector scanning the spin plane. This plane was close to the meridian plane near 1036-2236 local time. The component in the equatorial plane pointing to dayside is referred to as V_1. The component perpendicular to the equatorial plane and pointing to north is referred to as V_2. The effective energy range of TIDE covers only the low energy portion of the magnetosheath population. We have however developed a method to extrapolate the missing population and estimate the true moments. The details of the method will be discussed in the next section. The large negative values in V_2 and other anomolous readings during these intervals result from the instrument response to unshocked solar wind (which it was not designed to measure). We have kept these values because they mark intervals of solar wind encounters by POLAR, although they should not be interpreted quantitatively. The magnetic field was measured by the POLAR Magnetic Field Experiment (MFE) [*Russell et al.*, 1995].

Before 0530 UT, POLAR was clearly in the magnetosphere, and this period provides the reference magnetospheric field direction. Near 0945 UT, POLAR moved into the solar wind briefly as indicated by the sudden drop in the density, temperature and field strength. The temperature dips near 0740 UT and near 0920 UT were also associated with pairs of bow shock crossings as discussed by *Russell et al.* [2000]. These bow shock crossings are highlighted by arrowheads in panel seven. It is difficult to identify the location of the satellite for

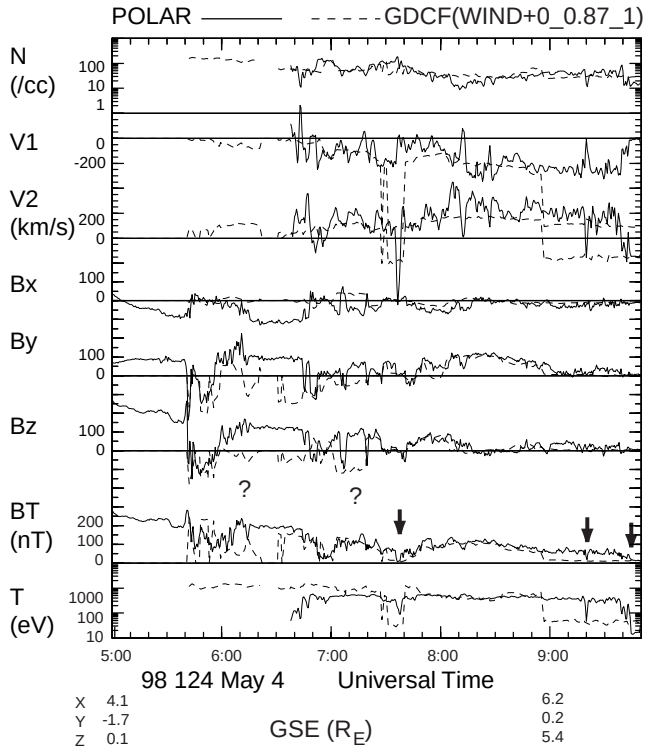

Figure 3. Comparison of POLAR measurements (solid lines) and the model predictions (dashed lines). From the top are the ion density, two components of the velocity in the spin plane of POLAR, three components, in GSE, and magnitude of the magnetic field, and the temperature. The POLAR density, velocity and temperature are based on TIDE measurements and are derived using the method discussed in section 3. The model predictions are based on WIND solar wind measurements and a vacuum dipole magnetosphere. The solar wind arrival time is same as the convection time from WIND to the Earth, the magnetosphere is reduced by 13 %, and the solar wind temperature has not been adjusted. Question marks indicate the periods when the identification is difficult using the magnetic field alone. Arrowheads indicate when bow shock crossings occurred.

some periods of strong positive B_Z, because the large B_Z may indicate possible magnetospheric field encounters, but may also be due to northward IMF intervals. Based on the magnetic field alone, it is relatively certain that POLAR was in the magnetosphere during the period from 0615 to 0640 UT. However it is challenging to identify the location of the satellite during the intervals of 0600-0610 UT and 0705-0715 UT, as marked by question marks, because the magnetic field in both intervals varied in a manner consistent with the magnetospheric field direction while the high-frequency fluctuations seem to belong to the magnetosheath. One of the purposes of this investigation is to determine the location of the satellite during these and other intervals from GDCF model predictions and particle observations.

We compare predictions of the GDCF model using each of the solar wind monitors and the two magnetopause models. For each case, we make many runs adjusting three parameters for a best overall fit. The three adjustable parameters are a time shift added to the simple convection time, a scale factor multiplying the standoff distance of the magnetopause in order for the predicted magnetopause location to be consistent with the observed crossing, and a scale factor multiplying the solar wind temperature. The temperature factor will affect the solar wind Mach number and hence the thickness of the magnetosheath. It is adjusted to match the bow shock location with the observed bow shock crossings. Detailed discussion and justification for the three parameters can be found in *Song et al.* [1999a, b]. For this study, they can be simply considered as calibration factors to produce the best agreement between the model prediction and reality. With these 3 adjustable quantities, the physics of the GDCF model provides the basis for the remaining predictions. By testing the model predictions against a large number of events, we can validate its usefulness and the range of the calibration factors. This event tests the model under extremely strong and perturbed solar wind conditions.

Since we have two solar wind monitors and two magnetopause models, there are four possible prediction models. In the following presentation we choose to present the models in the order of improved fit to the observed magnetic fields. The poorest fit is shown in Figure 3 which is based on the WIND solar wind measurements (dashed lines) in Figure 2 and the vacuum dipole field for the magnetopause. The three adjustable parameters are 0, 0.87, and 1. Namely, the time shift to the earth is the same as that obtained by dividing the distance to WIND along the sun-earth line by the solar wind speed, the standoff distance is 13 % closer to the earth than the dipole field model prediction, and the magnetosheath thickness is the same as that predicted by gas dynamics but using the magnetosonic Mach number to replace the Mach number in gas dynamics. The GDCF model does not predict magnetospheric values, which have been set to be zero for the field and velocity. Consistent with observations, the first magnetopause crossing occurred near 0540 UT

when the predicted field and measured field start correlating. However the model predicts a few multiple crossings which were not observed. As we discussed in the introduction, the GDCF model prediction provides a reference for the draped magnetosheath field under the assumptions discussed in detail by *Song et al.* [1999a]. The most important assumption to this part of the discussion is that the solar wind is uniform in a plane that intersects the sun-earth line. If the solar wind contains large-amplitude small-spatial-scale irregularities, it is not necessary that the model predictions represent the draped magnetosheath field. One may assume that when the observed field is very different from the predicted field in Figure 3, allowing for small adjustments in the timing, the satellite is in the magnetosphere or magnetopause current layer. In fact, we have made a few runs using smaller magnetopause distance factors, in order to provide the magnetosheath draped field without interruptions by the predicted magnetopause crossings. The correlation between the observation and prediction becomes poor at about 0600 UT, indicating that POLAR moved into the magnetopause and magnetosphere. From 0610 to 0650 UT, the satellite was in the magnetosphere because the observed field is nearly opposite to the prediction and is in the direction of, and with a similar strength to, the magnetospheric field. The model predicts a thinner magnetosheath than observed, as indicated by the longer duration of the predicted but not observed solar wind encounter and earlier predicted bow shock crossing. The predicted solar wind intervals are most easily identified by the lower temperature and large negative velocities. In fact we made runs with larger temperature factors which show better agreements with the observed bow shock crossings. We decide not to show these results because when using the *Shue et al.* [1998] model or using the ACE solar wind measurements, the thickness of the magnetosheath does not seem to be a major concern. Nevertheless, the observed and predicted fields show a relatively good correlation most of time. One exception is from 0750 to 0810 UT when the observation is somewhat different from the prediction. As we will show later in the paper, during this interval, POLAR was most likely to be in the magnetosphere or its boundary layers. The most interesting interval is from 0700 to 0720 UT. The observed field is nearly opposite to the predicted field and is in a similar direction to the magnetospheric field. Based on this run alone, one might conclude that POLAR was in the magnetosphere during this interval. However, as will be shown later, when using the ACE solar wind measurements and when examining the particle measurements, POLAR was most likely to be in the magnetosheath during the interval because the IMF direction measured by ACE is quite different from that measured by WIND as marked in Figure 2. The model predicts that POLAR was in the magnetosheath for times between 0610 UT and 0640UT but observations show that POLAR was in the magnetosphere. One can in principle further reduce the size of the magnetosphere using a smaller value of the magnetosphere size parameter. However, doing this will worsen the prediction of the bow shock location as well as the agreement with observations in the interval near 0800 UT when POLAR was in the magnetopause/boundary layer region.

Figure 4 compares the observations with GDCF model predictions based on the ACE solar wind measurements and with a vacuum dipole field model for the standoff distance similar to Figure 3. A time shift of 4 min is added to the simple convection time; namely, the solar wind needs to arrive later when using ACE for this event. This 4-min difference can be understood from Figure 2. The solar wind density structures arrived at ACE about 6 to 8 min earlier than at WIND. The distance in the x direction from ACE to WIND is 13 R_E, or 2 min which is already included in the model. The observed magnetopause standoff distance is again 13 % smaller than that predicted by a vacuum dipole magnetospheric field. Using the ACE solar wind measurements, clear improvement can be found in the locations of the bow shock and maybe the magnetopause. The broader region of magnetospheric field prediction by the model around 0630 UT and the bow shock location are both in better agreement with the observations. Furthermore, the predicted bow shock crossings near 0738 UT are improved slightly although the exact timings are not accurate. One is also able to see that the predicted magnetosheath draping field matches well with the observations from 0700 to 0720 UT, indicating that POLAR was in the magnetosheath during this interval. Here we recall that according to the WIND prediction, during the interval around 0710 UT, the draped magnetosheath field is quite different from the observed one. Therefore, this interval becomes important to test the model predictions and to decide which solar wind monitor is most likely to provide the upstream conditions that actually reached the magnetosheath at this time.

Figure 5 shows the GDCF predictions using WIND solar wind measurements and the *Shue et al.* [1998] model to determine the magnetopause standoff distance. The observed standoff distance is reduced by only 1 % from the *Shue et al.* [1998] model, indicating

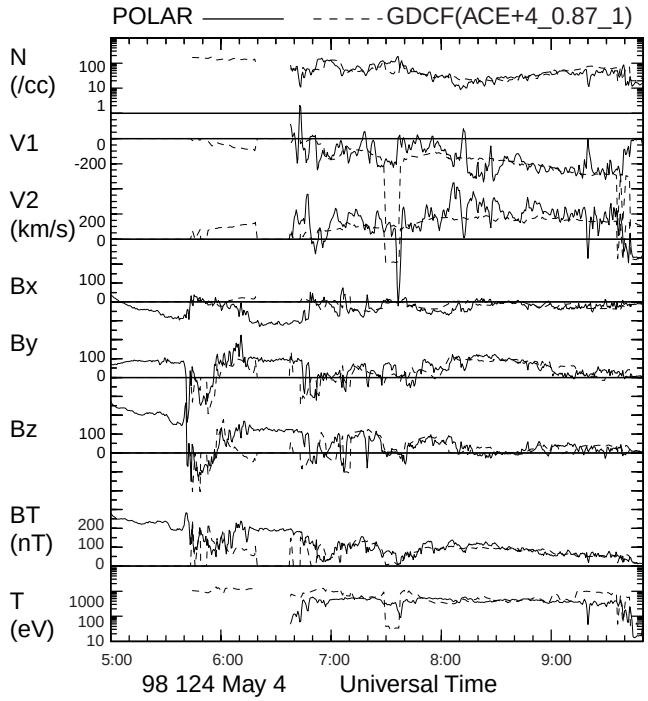

Figure 4. Comparison of the POLAR measurements and the model predictions using the ACE solar wind data and a vacuum dipole field model in the same format as Figure 3. The three adjustable parameters are 4, 0.87, and 1.

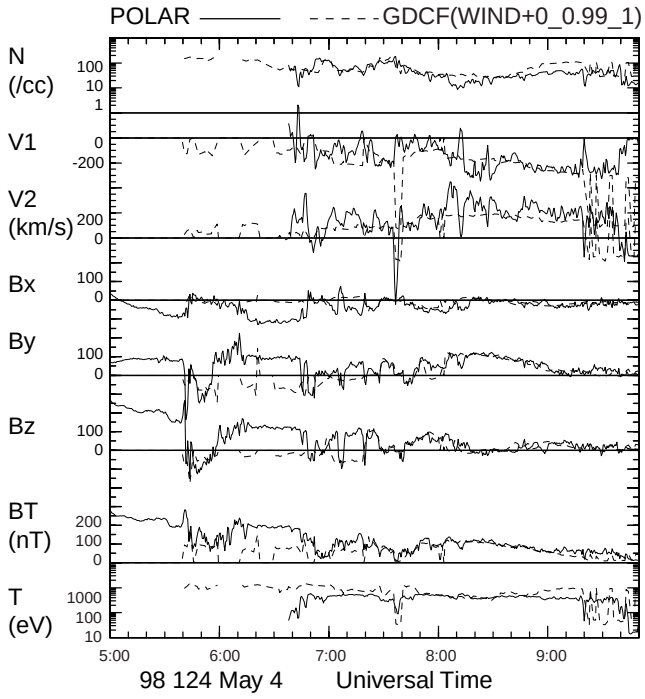

Figure 5. Comparison of the POLAR measurements and the model predictions using the WIND solar wind data and *Shue et al.* [1998] model in the same format as Figure 3. The three adjustable parameters are 0, 0.99, and 1.

that the *Shue et al.* [1998] model significantly improves the prediction of the magnetopause standoff location. No other adjustments are made. Compared with Figure 3, significant improvement is made in the predicted magnetopause and bow shock locations although neither is accurate. The prediction of the field is also somewhat better, for example, see B_y from 0810 to 0850 UT. Compared with Figure 4, the prediction during the interval around 0710 UT remains quite different from that predicted using the ACE solar wind measurements. However, Figure 5 shows nicely the agreement between the predicted and observed brief solar wind encounter near 0738 UT. Actually the timing and the duration of this pair of bow shock crossings are in the best agreement with observations among the four models we have examined. In addition, an interesting feature occurs near 0800 UT when the prediction indicates multiple magnetopause crossings. This interval will be taken as another critical interval in the evaluation.

The predictions using ACE solar wind measurements and the *Shue et al.* [1998] model are shown in Figure 6. The additional time shift is again 4 min and the standoff distance is 5 % smaller than the *Shue et al.* [1998] model. Compared with Figure 5, the magnetopause location prediction is slightly better. Near 0800 UT, magnetopause crossings are predicted. The timing of the solar wind variations after 0920 UT is better than Figure 5 but may not be as good as Figure 4. ¿From 0810 to 0850 UT, Figure 5 is better. The field direction for the solar wind period near 0738 UT is predicted more accurately than other methods, but there is an additional solar wind period near 0731 UT, which is not recorded in observations. In addition, there is a solar wind period predicted near 0700 UT, which is consistent with the POLAR magnetic field measured slightly earlier. As will be seen in the next section, particle measurements do not seem to support this prediction.

4. Particle Observations

To identify regions from POLAR observations is not trivial for this event because of the rapid large-amplitude changes in the solar wind and IMF and the rapid motions of the magnetopause and bow shock. In

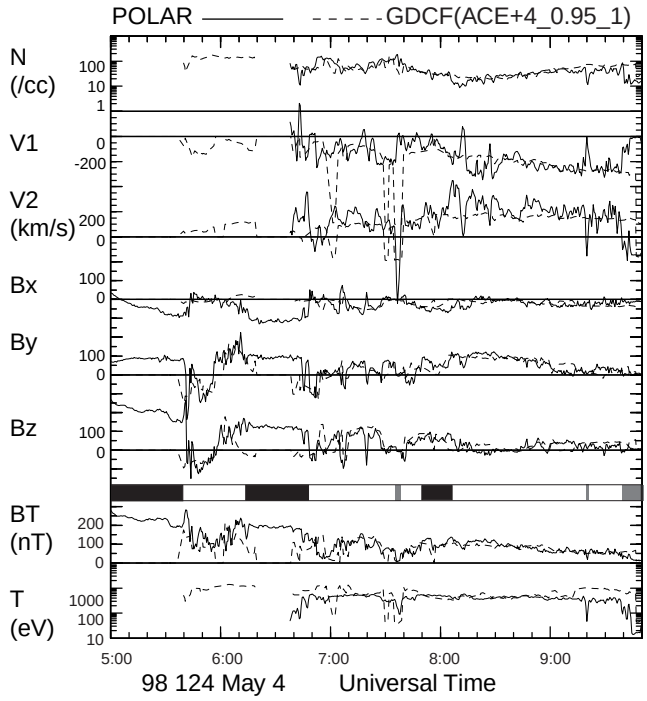

Figure 6. Comparison of the POLAR measurements and the model predictions using the WIND solar wind data and the *Shue et al.* [1998] model in the same format as Figure 3. The three adjustable parameters are 4, 0.95, and 1. In addition, the identification of regions in consideration of both model prediction and in situ observations is shown in the horizontal bars. Solid (shaded) bars indicate the periods of the magnetosphere (solar wind). The open bars, however, indicate either the magnetosheath or magnetopause current layer.

particular, there are periods when the magnetic field was in the direction of the magnetospheric field and had a relative large magnitude, and when the predictions depend on the solar wind monitor and magnetopause model used. We use here measurements from POLAR ion instruments (TIDE, TIMAS, and HYDRA) to help in region identification. Detailed inspections of the particle distribution functions are used as diagnostics of the plasma population.

4.1. Instruments

TIDE [*Moore et al.*, 1995] was designed to provide full 3- dimensional (3-D) ion composition measurements from 0 to 500 eV. The major advantages of TIDE to our study are its high sensitivity and the ability to detect extremely low energy ion particles. We recall that all particle instruments previously used in magnetopause/boundary layer/magnetosheath studies had relatively high lower-cutoff energies. For example, ISEE-FPE's lower-cutoff energy is 75 eV. The lower-cutoff energy for AMPTE/IRM was 20 eV while the distribution data was available only with a much lower time resolution. Therefore, the particle distributions in the range of eV to 10s of eV are largely unknown. TIDE provides the first opportunity to study eV to 10s of eV ions in this region. Although TIDE was originally designed to measure different species, the mass resolution sensors failed a few months after the launch and only 2-D measurements were transmitted after that. The time resolution of the 2-D measurements is a spin period which is 6 sec. The moments measurements shown in Figures 3 to 6 have been averaged to 1 min. The higher-cutoff energy, 500 eV, of TIDE limits the study to the ionospheric population and to the low energy portion of the magnetosheath plasma and magnetospheric population.

The Toroidal Imaging Mass-Angle Spectrograph (TIMAS) [*Shelley et al.*, 1995] on the Polar spacecraft can obtain full energy/pitch angle distributions for four ion species simultaneously (H^+, He^{++}, He^+ and O^+). TIMAS covers the energy range from 16 eV/e to 33 keV/e and provides a 98% coverage of the unit sphere during its 6-second spin period.

HYDRA [*Scudder et al.*, 1995] covers the energy range from 20eV to 20keV for ions (no composition). This measures the bulk of the magnetosheath populations.

4.2. Distribution Functions

Plate 1 shows the ion energy spectra from TIMAS, HYDRA and TIDE. The bulk of the magnetosheath population appears as an enhancement in the keV range. The bottom panel of Plate 1 shows flux as a function of the retarded potential measured by TIDE. The retarded potential is proportional to the energy if the satellite potential remains the same, versus time. The instrument did not start formal operation until 0640 UT. Because the TIDE instrument covers a very different energy range from instruments used in previous magnetopause/magnetosheath studies, the morphology of particle distribution functions at this energy range at each of the regions near the magnetopause and in the magnetosheath are not immediately clear. We need to utilize the knowledge acquired previously from other energy ranges along with the location predicted by the GDCF model to gradually understand each population, its origins and its functions. By carefully examining the distribution functions measured during the event,

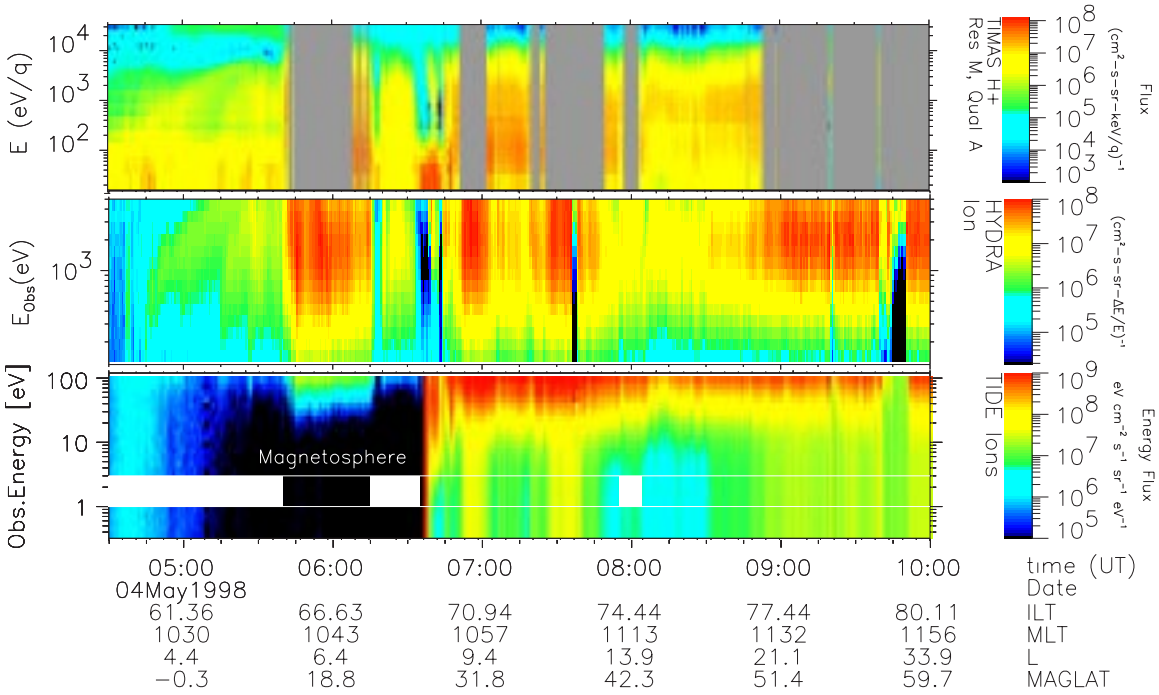

Plate 1. Spectrograms of ion energy flux from TIMAS, HYDRA, and TIDE during the May 4, 1998, event. The white bars in the bottom panel indicated the magnetosphere and boundary layer intervals.

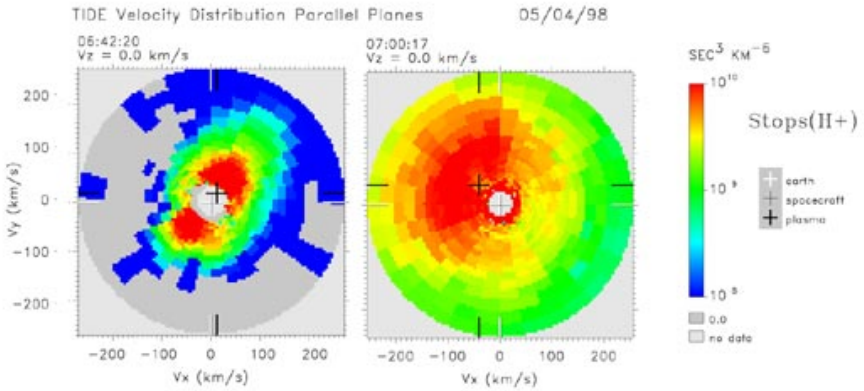

Plate 2. Two types of distribution functions seen during the May 4 by TIDE, 1998 event. The distribution shown in the left (right) panel is from the region identified as the magnetosphere (magnetosheath). The distribution function is measured in the satellite spin plane which is about in the 1100 local time meridian plane.

we have been able to identify three fundamentally different types of distributions. Two of them are shown in Plate 2. The left panel shows the distribution from the region identified as the magnetosphere according to the GDCF model, the magnetometer and particle measurements. The characteristic of this distribution function is the enhancement at the lowest energies and the void at higher energies. The ionosphere could be one source of ions [*Peterson et al.*, 1982]. Because the field is stronger at the ionosphere than at the dayside magnetopause, one would expect the ionospheric population to have a larger parallel temperature when observed at the dayside magnetopause. However, the temperature anisotropy is mostly perpendicular to the magnetic field, indicating that these ions are not moving along the geomagnetic field from the ionosphere. Cold magnetospheric ions drifted from the nightside are another possible source. The origin of this population remains

to be investigated. The right panel shows a distribution function from the region identified as the magnetosheath. Clearly, this distribution is much warmer with a subsonic speed. The flow is anti-sunward and northward. It is consistent with our understanding of the magnetosheath plasma flow when POLAR was above the equator. The measurements made during the solar wind intervals are quite distinct. However the instrument responses under such plasma conditions are not well understood and the data are not shown here.

The top panel of Plate 1 shows H^+ flux measurements by TIMAS. High count rates during the event drive the TIMAS detector into a nonlinear response range. However, this occurs only for events with very high count rates and for the energy range below 1 keV/e where the most intense fluxes are found. Furthermore, this nonlinearity is correctable by software and work is in progress to implement those modifications. The current software automatically suppresses periods where a nonlinear response occurs resulting in gaps in the TIMAS flux panel. These gaps clearly mark periods with exceptional high flux like the magnetosheath or cusp regions during the event. Most of the TIMAS data represent flux measurements in the magnetosphere and boundary layers with some brief encounter of the unshocked solar wind at about 07:37, 09:20 and 09:45 UT. While being in the magnetosheath most of the time POLAR was close to the magnetopause at around 08:00 UT. The TIMAS moments for that time period show that the plasma velocity in the x direction (GSE) dropped from about -200 km/sec in the magnetosheath to about zero. Three-dimensional cuts in velocity space show distributions typical for the magnetosheath boundary layer (MSBL) and LLBL as observed earlier by *Fuselier et al.* [1997].

The middle panel of Plate 1 shows the ion flux measured by HYDRA. The magnetosheath regions are identified with the enhancements in keV ions. The fluxes decreased significantly in the boundary layer regions. There are sharp drop-outs during the solar wind intervals.

Because the gyroradius varies with species and energy, the boundaries drawn from each instrument may differ. The identification of regions to be discussed in section 3.4 is based on the synthesis of these measurements.

4.3. Moment Estimates

To measure plasma moments, a detector needs to cover the majority of the phase space distribution of the plasma. While the moments from HYDRA are not available, TIDE covers only a small portion of the phase space. However, we have developed a method to derive the moments based on the finite energy coverage and the approximation of the plasma distributions being Maxwellian. We assume a convective Maxwellian distribution with a density N_0, velocity $\mathbf{V}_0$, and temperature T_0. A detector with a higher-cutoff energy E_0 measures a volume within a sphere in the phase space with a radius of $(2E_0/m_i)^{1/2}$ where m_i is the mass of the particles. For a Maxwellian distribution, one can extrapolate the population beyond this sphere. Therefore, the moments of the plasma can be derived from the measured portion within the sphere. The mathematical expressions have been derived by *Song et al.* [1997] who solved the reverse problem when an instrument has a large lower-cutoff energy. Therefore, the application to our problem is then to take the missed population in *Song et al.* [1997] as the measured population. Figure 7 shows the results for the TIDE measurements. The density, velocity, temperature, and pressure are calculated based on the population below 500 eV of a Maxwellian distribution. These quantities are then normalized by the density, velocity, temperature, and pressure, respectively, calculated from the whole Maxwellian distribution. This is done as functions of theoretical temperature and velocity. As we see from the figure, the moments derived by summation of the distributions measured by TIDE will always underestimate the true moments. (Here we recall that if an instrument does not measure particles of lowest energies as usually is the case in magnetospheric particle instruments, a quantity may be either over- or under- estimated depending on the plasma conditions [*Song et al.*, 1997].) In general, when the temperature or velocity of the plasma increases, the population that is measured by TIDE decreases. When the temperature is greater than 10^7 K (or 1000 eV) or when the velocity is greater than 300 km/s, TIDE will measure only a small fraction of the population and have a very large uncertainty. The effect on the pressure is the largest and equals the product of errors in the density and in the velocity. Here we recalled that in the case when the lowest energy particles are not observed, the pressure has the least error. The effect on the temperature is the same as that on the velocity. As shown in Plate 2, the distribution function in the magnetosheath may be approximated by a Maxwellian within the TIDE coverage. Therefore, our application will be restricted to the magnetosheath region. Based on the prediction from the GDCF model, the temperature of the magnetosheath plasma is about 500-1000 eV and the velocity about 200 km/s. The mo-

ments measured by TIDE need to be multiplied by a factor of 3-5. The observed values shown in Figures 3 to 6 have used a factor of 5 to scale the density, velocity, and temperature. As can be seen in these figures, these values are in reasonable agreement with the predicted values in the magnetosheath.

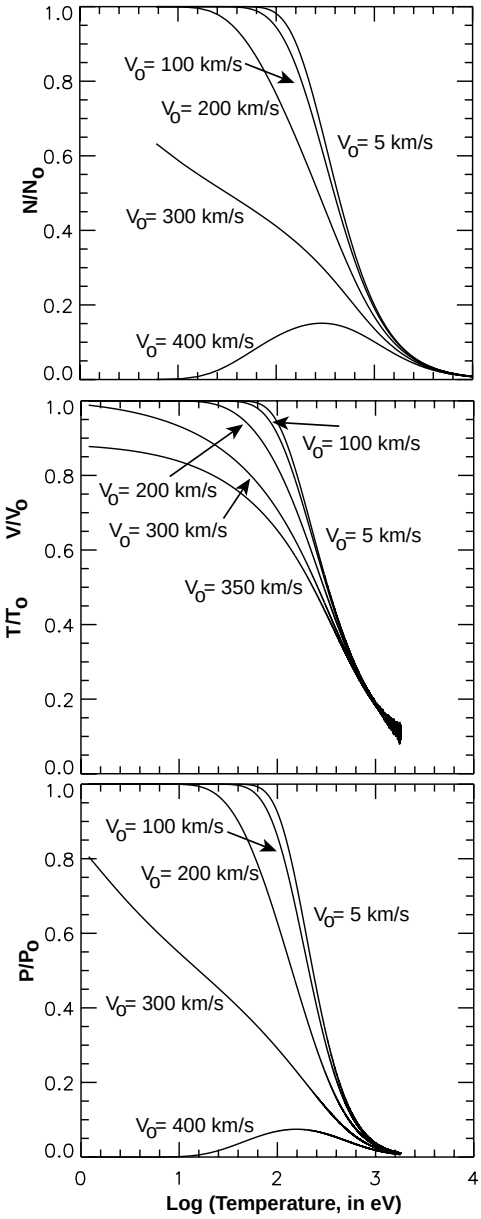

Figure 7. Effects of the higher cutoff energy of TIDE on the moments measurements as functions of the temperature and velocity of the plasma. The apparent moments are normalized by the theoretical values.

4.4. Region Identification

As we discussed in section 2, identifying the location of the satellite, using the magnetic field alone, is difficult for some periods, in particular when the field is in a similar direction and magnitude to the magnetospheric one. Relying on plasma measurements alone for identification, on the other hand, may also be ambiguous because there are several different possible processes depending on the satellite location relative to the possible reconnection sites and because of the spatial-temporal ambiguity. For example, the interpretation of a particle feature near the magnetopause depends significantly on the IMF orientation. When the IMF rotates rapidly and frequently, the IMF conditions under which the particle feature is observed can be ambiguous. Here we recall that the solar wind arrival time cannot be handled accurately without using the sheath magnetic field measurements. The satellite location within the boundary layer during this event is particularly difficult to determine because the variations are rapid and, more importantly, the measurements from the two solar wind monitors are different sometimes. The GDCF model prediction provides an additional constraint to further reduce the uncertainty in the solar wind timing. We synthesize the information obtained from both field and particle measurements and the model predictions. We compare the predicted draped sheath field with the observed field and take into consideration the predicted location of POLAR, which will be discussed in the next section. The solar wind periods can be identified unambiguously from TIDE particle measurements because the solar wind distribution is out of the range of the TIDE coverage. TIDE covers only the low energy range of the magnetosheath and magnetospheric particles. The magnetosheath population can be identified with a relatively broad distribution. Because of the finite energy coverage, however, when the solar wind density changes with very large amplitude, using TIDE alone, there is a possible ambiguity in distinguishing the regions with denser cold plasma during low solar wind density periods from the regions of warm plasmas during enhanced solar wind density. HYDRA was best situated to measure the magnetosheath population. TIMAS covers well the high-energy portion of the distributions and is sensitive to the magnetospheric population. Ambiguity occurs in the vicinity of the magnetopause boundary layer. We examine the details of the distribution functions in these regions to make our identifications.

We identify the regions during this event and use the bar coding in Figure 6 to show the identification.

Here we remark that the field in the magnetopause current layer can be either similar to, or different from, the draped sheath field. POLAR was in the magnetosphere before 0540, and reentered it between 0615 and 0648 UT. There are transient signatures near 0545 UT and near 0645 UT which are most likely associated with partial magnetopause crossings. POLAR moved into the solar wind between 0736 and 0738 UT. Near 0733:40 UT, the signatures indicate partial bow shock crossings. The signatures near 0800 UT are very interesting and most difficult to identify. The magnetometer measurements indicate POLAR was in the magnetopause current layer or magnetospheric field from 0750 to 0755 UT and near 0805 UT. TIDE measurements indicate that the particles are most likely of magnetosheath type. TIMAS measurements show particles of cusp characteristics. Therefore, POLAR was most likely to be near the magnetopause current layer or the LLBL. POLAR encountered the solar wind briefly near 0920 UT and entered the solar wind after 0939 UT.

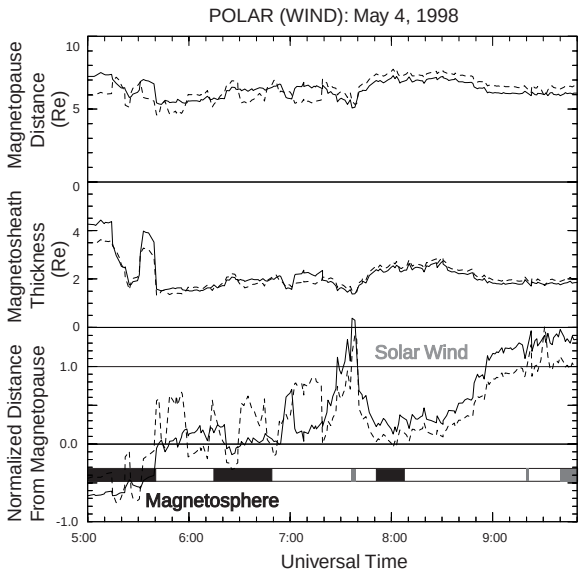

Figure 8. Predictions of the distance of the magnetopause, thickness of the magnetosheath and the distance from the magnetopause to POLAR normalized by the magnetosheath thickness. The predictions are based on WIND solar wind measurements and use the same parameters as in Figures 3 and 5. Solid (dashed) lines are predicted using a vacuum dipole field (*Shue et al.* [1998]) model. All quantities are evaluated along the direction from the Earth to POLAR. In the normalized distance, the magnetopause is at zero and the bow shock is at 1. The bar coding indicates the location of POLAR in the format as in Figure 6.

5. Location of POLAR

The location of the satellite relative to the magnetopause and bow shock is most critically dependent on the magnetopause model. The thickness of the magnetosheath is proportional to the magnetopause standoff distance [*Petrinec and Russell*, 1995] and depends on the solar wind magnetosonic Mach number. When the Mach number is large as is typical of the solar wind, the Mach number dependence is very weak.

Figures 8 and 9 show the magnetopause distance, the thickness of the magnetosheath and the relative location of POLAR from the magnetopause to the bow shock using the WIND and ACE solar wind measurements, respectively. All quantities are derived in the direction from the earth to the satellite. The solid (dashed) lines show the results using the vacuum dipole field (*Shue et al.* [1998]) magnetopause model. The differences in the magnetopause distance variations between the solid and dashed line in the top panel of each figure are caused mainly by the IMF B_Z effect, and are bigger during southward IMF periods. The solid lines contain only effects of the dynamic pressure. The magnetosheath thickness is well correlated with the magnetopause distance. This is because in gas dynamics, the magnetosheath thickness is proportional to the standoff distance. The magnetosheath thickness also depends on the Mach number. In our model calculation, the Mach number used is the magnetosonic Mach number. Therefore the strength of the magnetic field also affects the thickness of the magnetosheath, but to a lesser degree.

In the course of this investigation, we have made many runs using different sets of parameters. When using a smaller size of the magnetosphere, the model provides the draped magnetosheath field, which can be used to compare with the observations and to distinguish magnetospheric periods from magnetosheath periods. A major advantage of our method is that the magnetopause and bow shock motions and magnetosheath fluctuations can be traced back in the solar wind. In the following we summarize our understanding of the event based on these runs.

The first magnetopause crossing at 0540 UT was triggered by the density enhancement near 0510 UT, in Figure 2. Here we note that although the IMF turned southward 8 min earlier with a very large strength, the southward IMF alone did not cause enough magnetopause erosion for a POLAR magnetopause crossing. The second magnetopause crossing, when POLAR

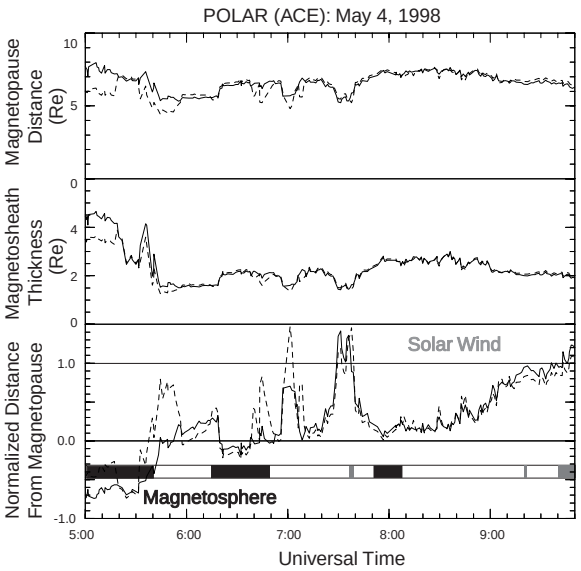

Figure 9. Predictions of the distance of the magnetopause, thickness of the magnetosheath and POLAR location in the same format as Figure 8. The predictions are based on ACE solar wind measurements.

moved back into the magnetosphere, was caused by the drop in the solar wind density. The predictions made from WIND data have very large errors in timing of the first density enhancement although they are good in other features later. Therefore the solar wind seen near the earth is more likely to come from the ACE location. POLAR moved back into the magnetosphere near 0600 UT, when it was in the magnetopause current layer. The location of POLAR during the first magnetosheath encounter would be best represented by the *Shue et al.* [1998] model using ACE upstream values.

The magnetopause crossing at 0650 UT was caused by the secondary peak in the solar wind density near 0620 UT. As we discussed earlier, the ACE and WIND measurements have a major difference in B_Z during this magnetospheric interval. Based on POLAR measurements, the solar wind seen near the earth is again most likely to come from the ACE location. For the magnetospheric interval, the vacuum dipole field model with an additional time shift of zero rather than 4 min, seems to do a better job because it predicts that POLAR does not move into the sheath very far. Here we recall that purpose of the time shift is to align the predicted field variations with observed ones. The *Shue et al.* [1998] model predicts a large amplitude magnetopause motion which does not seem to be observed. Different polarities of IMF Bz are measured by the two solar wind monitors during the secondary density peak near 0620-0630 UT. Note that the timing and duration of this feature in the magnetic field are similar at the two monitors. However, the arrival times of the density enhancement at the two locations differ by 5 min. ACE measured a negative B_Z and WIND measured a positive B_Z during the density peak. This difference cannot be resolved using the magnetosheath field measurements because of the rapid reversals of the field near the feature. Only the *Shue et al.* [1998] model, using ACE data, predicts bow shock crossings during the interval, but the POLAR plasma measurements do not support this possibility.

The biggest solar wind density enhancements occurred near 0700 UT. The timing and shape of the enhancements are different as recorded by the two solar wind monitors. The last peak in the density in each monitor is responsible for the bow shock crossings near 0738 UT by POLAR. All four methods predict solar wind encounters although the details are different. Overall, the *Shue et al.* [1998] model using WIND data seems to provide the best prediction surrounding this interval. Notice that the predictions using the WIND solar wind measurements are generally better than that using ACE after 0720 UT, indicating that after 0720 UT (sheath time) the solar wind was more likely to come from WIND.

The magnetopause/boundary layer encounter near 0800 UT by POLAR was due to the solar wind velocity drop near 0720-0730 UT, following decrease to more normal values. There are a few data gaps in the ACE data. Nevertheless, all methods predict that POLAR was very close to the magnetopause and some predict magnetopause crossings.

After 0750 UT (sheath time), the solar wind dynamic pressure increased more gradually, which caused the magnetopause and bow shock to move inward, while POLAR continued its outbound path. The POLAR bow shock crossings near 0920 UT were triggered by a small solar wind velocity peak in WIND data near 0810 UT, which was not observed by ACE, in Figure 2. However, based on WIND measurements, there should have been a few more bow shock crossings before the main crossing at 0950 UT. The POLAR observations for the interval from 0810 to 0950 UT would be best predicted by the vacuum dipole field using the WIND data if the magnetosheath is 40 % thicker (not shown).

6. Discussion

We have provided detailed analysis of the event during which the POLAR satellite crossed the dayside magnetopause and then the bow shock for the first time,

on May 4, 1998. Both WIND and ACE were more than 200 R_E upstream in the solar wind. Although they were separated by only about 50 R_E in the direction perpendicular to the solar wind, they sometimes observed significantly different solar wind features or different forms of the same features. Both solar wind and IMF were highly perturbed during the event. The temporal and spatial variations in the solar wind make the studies of this event extremely challenging. Furthermore, the solar wind variations caused the magnetopause and bow shock to move rapidly over large distances; making interpretation of the POLAR measurements near the magnetopause/boundary layer and in the magnetosheath even more difficult. However, this provides us a rare opportunity to test our understanding and prediction capability of the magnetopause and magnetosheath. We use the GDCF model to predict the magnetosheath reference quantities and the POLAR location relative to the magnetopause and bow shock. We have performed such predictions using both the ACE and WIND solar wind measurements and both a dipole field and an empirical magnetopause model. The model predictions provide: (1) a solar wind arrival time that varies with the solar wind speed, (2) reference values of magnetosheath quantities with a known systematic formalism, and (3) the changing location of POLAR with respect to the magnetopause and bow shock as the solar wind and IMF vary. Although the model prediction is not completely self-consistent, it is systematically conducted throughout the event. When comparing the predictions with observations, the ambiguity in the interpretation of the observations can be significantly reduced. Using this method, observed features in the magnetosheath and near the magnetopause can be traced back to the solar wind. This analysis provides a baseline for other POLAR studies of this event.

The TIDE instrument provides the measurements in the dayside region from the solar wind to the magnetosphere. These measurements cover the low energy range of the plasma which has not been studied previously. The magnetospheric population contains a very cold component the temperature of which is much higher in the direction perpendicular to the magnetic field during the event. The source of this component is not immediately clear and remains to be investigated. Since this event was produced by some unusual upstream conditions when POLAR was very close to the earth, the cold plasma was actually observed at a small radial distance. It is not clear from this case alone whether this population is associated with processes that occur under this extreme solar wind condition or if this is a population commonly present at small radial distances. As the apogee of the POLAR orbit drifts down to low latitudes, TIDE will have more opportunities to sample the dayside magnetopause and outer magnetospheric regions under various upstream conditions. We will then be able to assess the conditions for the presence of such a population. Although TIDE with its limited energy coverage samples only a small portion of the magnetosheath distribution, we have developed and demonstrated a technique that can extrapolate from the observed population to derive the plasma moments in the magnetosheath.

To assess the performance of a model is not a simple task. There are two major criteria, accurate prediction of the large temporal scale magnetopause-bow shock locations and of their small temporal scale variations. This whole event lasted about 7 hours. We have discussed in detail the first part of the event. If one looks at the overall prediction throughout the 7-hour interval, the *Shue et al.* [1998] magnetopause model performs better than the vacuum dipole field model. Using the vacuum dipole model, the standoff distance of the magnetopause needs to be significantly smaller than the model prediction. It is slightly bigger at the early times than in the later times (which are not shown in this paper). Therefore a single constant magnetopause scale factor is not sufficient to describe the magnetopause standoff distance for the 7 hours. The *Shue et al.* [1998] model, on the other hand, handles the magnetopause and bow shock locations reasonably well using a single constant magnetopause scale factor throughout the 7-hour period. However, if one looks into the details of the predictions, the *Shue et al.* [1998] model predicts some transient large spatial scale movements of the magnetopause and bow shock, some of which are not well supported by the POLAR observations, in particular the three peaks from 0640 to 0710 UT in the dashed line of the bottom panel of Figure 9. The *Shue et al.* [1998] model predicts that when the IMF is strong and southward, the magnetopause location will move much further inward than observed during these brief southward turnings. Meanwhile, because the obstacle becomes smaller, the thickness of the sheath also reduces. These two effects lead to outward motion of the satellite in a frame of reference at rest to the magnetopause. Therefore, brief southward turnings result in spikes in the normalized satellite location. However, observations indicate that sometimes the magnetopause does not seem to respond to the IMF changes at these small time scales. The differences in the performance of the models at different time scales lead us to con-

clude that the erosion of the magnetopause in response to southward IMF does not take place instantaneously and the preconditioning of the magnetosphere is important in such responses. Improvements may be found in the *Shue et al.* [1998] model predictions if the average of the earlier IMF directions, say, 10 to 20 min before the prediction time, is used.

This event also provides a unique opportunity to assess the evolution of spatial variations. Although the upstream conditions changed rapidly with large amplitudes, there often exists very good correlation between the predictions and magnetosheath observations. We have shown in section 4 that one is able to trace back most solar wind features and their influences on the magnetopause and bow shock locations and the magnetosheath quantities. Previously, *Song et al.* [1999b] documented a few other cases which coverd a variety of solar wind conditions. The predictability shown in these cases provides the justification for using the solar wind monitors at sun-earth liberation (L1) point to forecast the upstream conditions for the magnetosphere. We conclude that most of the time there are good correlations between the solar wind at L1 point and in the magnetosheath.

Sometimes the solar wind measured at a solar wind monitor location does not propagate to the earth's environment or it can evolve significantly from where it is monitored. The differences between what is measured by a solar wind monitor and what is expected at the earth's magnetosphere can sometimes cause major differences in the interpretation of the observations near the earth. We should comment here that small-scale large-amplitude solar wind structures do exist once in a while. However most of the time the correlation between the solar wind monitors and the magnetosheath observations is quite good. Therefore one should not interpret a near earth observation solely based on the unpredictability of solar wind conditions. One should also avoid the other extreme to interpret an observation based on unphysical arguments in order to satisfy the observed solar wind conditions. It is expected that small-scale large-amplitude structures are more likely to occur during highly disturbed days such as the May 4, 1998 event. In fact this is one of the largest disturbed days on record.

7. Conclusions

We have made predictions of the magnetosheath and bow shock under extreme solar wind conditions based on the GDCF model. Two solar wind monitors and two magnetopause models are used in the predictions. The preditions are compared with the POLAR in situ observations. The vacuum dipole magnetic field model significantly over-estimates the size of the magnetosphere. When it is properly scaled, the model reasonably describes the magnetosphere responses to small time-scale IMF fluctuations. The empirical magnetopause model, on the other hand, describes very well the magnetopause location in time-sclaes greater than 20 min. It has a tendency to over-estimate the magnetopause responses to brief southward turnings of the IMF. The modified GDCF model describes successfully the bow shock location and the magnetosheath quantities. The method used in the study provides a one-to-one correlation between the solar wind features and the magnetosheath conditions as well as the magnetopause and bow shock movement. The location of a satellite in this region can be determined. During the event, the two solar wind monitors occasionally observed quite different upstream conditions in short time-scales. The conditions near the earth can be traced back to one of the monitors. Which location better forecasts the near earth environment may depond on the orientation and evolution of the solar wind irregularities.

In connection with comparison of the model prediction with observation, we developed a method to derive the ion moments by extrapolating the distribution functions beyond the higher-cutoff energy of the TIDE instrument. This technique remains to be further tested in more events. The low energy particles measured by TIDE represent a new energy regime which has not been measured before in magnetopause studies. The magnetosheath low energy population appears to be the extension of the same plasma population observed at higher energies. There is an enhanced flux at the lowest energies on the magnetospheric side of the magnetopause boundary. This population has not been reported before in magnetopause studies. It has a much higher temperature perpendicular to the magnetic field. The origin of this population remains to be investigated.

Acknowledgments. The work at UM was supported by NASA under The UM Corperate Agreement NCC8-84, by NSF under Award NSF-ATM9729775, and by NSF-ONR under Award NSF-ATM9713492. The work at UCLA was supported by NASA under research grant NAG5-7721. The work at GSFC was supported by ISTP Project under UPN 370-17-43. The work at Los Alamos National Laboratory was conducted under the auspices of the US Department of Energy with support from NASA. The HYDRA results of this paper are the results of NASA funding under grant

number NAG 5 2231 and German DARA funding under grant 50 OC 8911 0.

References

Fuselier, S.A., B.J. Anderson and T.G. Onsager, Electron and ion signatures of field line topology at the low-shear magnetopause, *J. Geophys. Res., 102,* 4847, 1997.

Kuznetsov, S. N., and A. V. Suvorova, An empirical model of the magnetopause for broad ranges of solar wind pressure and B_z IMF, in *Polar Cap Boundary Phenomena*, edited by J. M. et al., p 51, Kluwer Acad., Norwell, Mass, 1998.

McComas, D. J., S. J. Bame, P. Barker, W. C. Feldman, J. L. Phillips, P. Riley, and J. W. Griffee, Solar wind electron proton alpha monitor (SWEPAM) for the Advanced Composition Explorer, *Space Sci. Rev.*, *86*, 563, 1998.

Moore, T. E., et al., The thermal ion dynamics experiment and plasma source instrument, *Space Sci. Rev*, *71*, 409, 1995.

Ogilvie, K. W., and G. K. Parks, First results from WIND spacecraft: An introduction, *Geophys. Res. Lett.*, *23*, 1179, 1996.

Peterson, W. K., E. G. Shelley, G. Haerendel, and G. Paschmann, Energetic ion composition in the subsolar magnetopause and boundary layer, *J. Geophys. Res.*, *87*, 2139, 1982.

Petrinec, S. M., and C. T. Russell, *Adv. Sp. Res.*, *18*, 1995.

Petrinec, S. M., and C. T. Russell, Near-Earth magnetotail shape and size as determined from the magnetopause flaring angle, *J. Geophys. Res.*, *101*, 137, 1996.

Roelof, E. C., and D. G. Sibeck, Magnetopause shape as a bivariate function of interplanetary magnetic field b_z and solar wind dynamic pressure, *J. Geophys. Res.*, *98*, 21,421, 1993.

Russell, C. T., R. C. Snare, J. D. Means, D. Pierce, D. Dearbourne, M. Larson, G. Barr., and G. Le, The GGS/POLAR magnetic field investigation, *Space Sci. Rev*, *71*, 563, 1995.

Russell, C. T., G. Le, P. Chi, X.-W. Zhou, J. H. Shue, S. M. Petrinec, P. Song, F. R. Fenrich, and J. G. Luhmann, The extreme compression of the magnetosphere, May 4, 1998, as observed by the POLAR spacecraft, *Adv. Space Res.*, *25*, 1369, 2000.

Scudder, J., et al., Hydra - a 3-dimensional electron and ion hot plasma instrument for the POLAR spacecraft of the GGS mission, *Space Sci. Rev*, *71*, 459, 1995.

Shelley, E. G., et al., The toroidal imaging mass-angle spectrograph (TIMAS) for the POLAR mission, *Space Sci. Rev*, *71*, 497, 1995.

Shue, J.-H., P. Song, C. T. Russell, J. K. Chao, and Y.-H. Yang, Toward predicting the position of the magnetopause within geosynchronous orbit, *J. Geophys. Res.*, *105*, 2641, 2000.

Shue, J. H., P. Song, C. T. Russell, J. T. Steinberg, J. K. Chao, G. Zastenker, O. L. Vaisberg, S. Kokubun, H. J. Singer, T. R. Detman, and H. Kawano, Magnetopause location under extreme solar wind conditions, *J. Geophys. Res.*, *103*, 17,691, 1998.

Smith, C. W., J. Leureux, N. F. Ness, M. H. Acuna, L. F. Burlaga, and J. Scheifele, The ACE magnetic fields experiment, *Space Sci. Rev.*, *86*, 613, 1998.

Song, P., X. X. Zhang, and G. Paschmann, Uncertainties in plasma measurements: Effects of lower cutoff energy and spacecraft charge, *Planet. Space. Sci*, *45*, 255, 1997.

Song, P., C. T. Russell, T. I. Gombosi, J. R. Spreiter, S. S. Stahara, and X. X. Zhang, On the processes in the terrestrial magnetosheath, 1: Scheme development, *J. Geophys. Res.*, *104*, 22,345, 1999a.

Song, P., C. T. Russell, X. X. Zhang, T. I. Gombosi, , and S. S. S. J. R. Spreiter, On the processes in the terrestrial magnetosheath, 2: Case study, *J. Geophys. Res.*, *104*, 22,357, 1999b.

Spreiter, J. R., and S. S. Stahara, A new predictive model for determining solar wind-terrestrial planet interaction, *J. Geophys. Res.*, *85*, 6769–6777, 1980.

Trattner, K. J., S. A. Fuselier, W. K. Peterson, S.-W. Chang, R. H. W. Friedel, and M. R. Aellig, Origins of energetic ions in the cusp, *J. Geophys. Res.*, *105*, 2000, submitted.

M. O. Chandler, NASA Marshall Space Flight Center, Huntsvill, AL 35812

R. H. W. Friedel, D. J. McComas, Los Alamos National Laboratory, Mail Stop D436, Los Alamos, NM 87545. (friedel@lanl.gov; dmccomas@lanl.gov)

J. U. Kozyra, Space Physics Research Laboratory, University of Michigan, Ann Arbor, MI 48109-2143. (JUKozyra@umich.edu)

R. P. Lepping, T. E. Moore, K. W. Ogilvie, NASA Goddard Space Flight Center, Greenbelt, MD

W. K. Peterson, K. J. Trattner, Lockheed-Martin ATC, 3251 Hanover Dr., L9-42, B255, Palo Alto, CA 94304-1191. (trattner@mail.spasci.com)

C. T. Russll, Institute of Geophysics and Space Physics, University of California, Los Angeles, CA 90095. (ctrussell@igpp.ucla.edu)

J.-H. Shue, Applied Physics Laboratory, The Johns Hopkins University, 11100 Johns Hopkins Road, Laurel, MD 20723-6099. (shuej1@oval.jhuapl.edu)

P. Song, Department of Environmental, Earth and Atmospheric Science and Center for Atmospheric Research, University of Massachusetts Lowell, 600 Suffolk Street, Lowell, MA 01854. (paul_song@uml.edu)

Received xxxx; revised xxxx; accepted xxxx.